Acta Mech Sin (2015) 31(3):338–348
DOI 10.1007/s10409-015-0462-1

RESEARCH PAPER

A new thermo-elasto-plasticity constitutive theory for polycrystalline metals

Cen Chen[1] · **Qiheng Tang**[1] · **Tzuchiang Wang**[1]

Received: 29 December 2014 / Revised: 17 April 2015 / Accepted: 23 April 2015 / Published online: 26 May 2015

Abstract In this study, the behavior of polycrystalline metals at different temperatures is investigated by a new thermo-elasto-plasticity constitutive theory. Based on solid mechanical and interatomic potential, the constitutive equation is established using a new decomposition of the deformation gradient. For polycrystalline copper and magnesium, the stress–strain curves from 77 to 764 K (copper), and 77 to 870 K (magnesium) under quasi-static uniaxial loading are calculated, and then the calculated results are compared with the experiment results. Also, it is determined that the present model has the capacity to describe the decrease of the elastic modulus and yield stress with the increasing temperature, as well as the change of hardening behaviors of the polycrystalline metals. The calculation process is simple and explicit, which makes it easy to implement into the applications.

Keywords Thermo-elasto-plasticity constitutive theory · Yield stress · Hardening behaviors · Finite temperature

1 Introduction

Polycrystalline metals have been investigated widely for many years, as they are important materials for the aerospace, energy, and chemical processing industries. Also, their material response at different temperatures has drawn the extensive attention of researchers. The results of experimental investigations [1–8] have determined that the yield stress and hardening of polycrystalline metals decreases with the increase in temperature at the same strain rate.

In previous years, theoretical models for polycrystalline plasticity have been developed. For example, the classic Taylor [9], self-consistent [10], and crystal plasticity finite-element models [11] have made significant progress from both macro and micro angles. First of all, the classic Taylor model [9] assumes that all grains must accommodate the same plastic strain, which is equal to the macroscopic strain and neglects the interaction between crystals. Therefore, it is more applicable for the face centered cubic (FCC) and body centered cubic (BCC) metals due to their crystallographic symmetry [12–14]. The next models are those based on the self-consistent approach. These models have been applied in the hexagonal close packed (HCP) [10,15] and other polycrystalline materials [16] for many decades. These models have the ability to describe the stress and strain variations from one grain to another and the interaction among the grains for the low crystallographic symmetry in polycrystals [17–19]. Moreover, new research has revealed that the self-consistent approach could potentially be implemented into the complicated loading condition deformation process [20], thereby describing the visco-plastic deformation using the dislocation-density constitutive law [21]. Lastly, the crystal plasticity finite-element models have been used to investigate the effects of the dislocation creep [22,23], hardening behavior [24], and crystal orientation [25] on the plastic behavior of metals at various temperatures. This model offers various constitutive formulations at the elementary shear system level, and can be applied easily into complicated boundary conditions [11].

In addition to the above mentioned theories, some new models have been proposed in recent years [26–32]. For example, the Johnson–Cook model [27], Zerilli–Armstrong

✉ Tzuchiang Wang
tcwang@imech.ac.cn

[1] State Key Laboratory of Nonlinear Mechanics, Institute of Mechanics, Chinese Academy of Sciences, 100190 Beijing, China

model [28], and Khan–Huang–Liang model [29–32]. These models have improved the constitutive descriptions of the dynamic plasticity of metals and have described the strain, strain-rate, and temperature relations for metals in large strain and high strain-rate regimes. The above models have all played important roles in the investigation of thermo-elasto-plastic deformations for polycrystalline metals. However, none of them have accounted for the thermal expansion in the deformation histories, which limits their applications to structural calculation with some boundary constraints. At the same time, we also need concise descriptions to reflect the temperature effects on the yield stress and hardening behaviour.

In this study, we propose a thermo-elasto-plasticity constitutive theory to describe behaviors of polycrystalline metals at different temperatures. First of all, a new decomposition of the deformation gradient is presented, and then the thermo-elasticity constitutive equation for single crystals is established. This is followed by obtaining the polycrystal elastic constants from single crystal elastic constants through integral transformation. The next focus is a macroscale plastic constitutive equation implementation to obtain the plastic deformation of the polycrystal. In the calculation process, a simple exponential relationship is proposed in order to describe the decrease of the yield stress with temperature increases, so that a law change of the material behaviour can easily be obtained. Lastly, the comparisons between the calculated and experimental results are presented.

2 Thermo-elasto-plasticity constitutive relationship for single crystals

2.1 Decomposition of the deformation gradient

In this paper, a new decomposition of deformation gradient is proposed to describe the thermo-elasto-plasticity deformation behavior, which is different from the kinematical theory [33–35]. As shown in Fig. 1, the whole deformation process is decomposed into four parts: the initial configuration at the undeformed state of 0 K (Fig. 1a), the first intermediate configuration after free thermal expansions at T K (Fig. 1b), the second intermediate configuration after elastic deformation at T K (Fig. 1c), and the current configuration after plastic deformation at T K (Fig. 1d).

The total deformation gradient is decomposed as

$$\boldsymbol{F} = \boldsymbol{F}^{\mathrm{p}}\boldsymbol{F}^{\mathrm{e}}\boldsymbol{F}^{*}, \tag{1}$$

where $\boldsymbol{F}^{\mathrm{e}}$ is the elastic deformation gradient, $\boldsymbol{F}^{\mathrm{p}}$ is the plastic deformation gradient, and $\boldsymbol{F}^{*}$ is the thermal deformation gradient due to the free thermal expansion.

The thermal strain tensor $\boldsymbol{E}^{*}$, elastic strain tensor $\boldsymbol{E}^{\mathrm{e}}$, and plastic strain tensor $\boldsymbol{E}^{\mathrm{p}}$ take the respective forms as

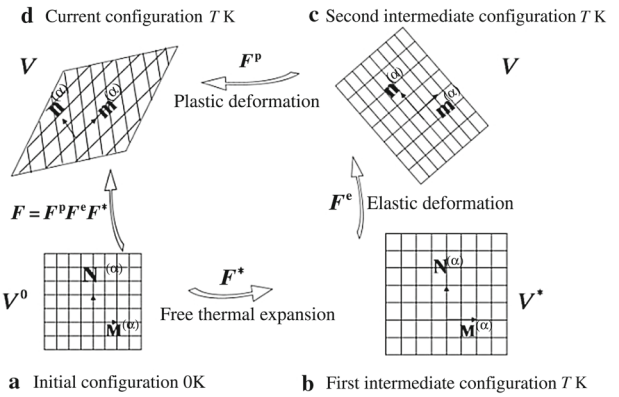

Fig. 1 Decomposition of deformation configuration. **a** Initial configuration. **b** First intermediate configuration. **c** Second intermediate configuration. **d** Current configuration

$$\boldsymbol{E}^{*} = \frac{1}{2}\left(\boldsymbol{F}^{*\mathrm{T}}\boldsymbol{F}^{*} - \boldsymbol{I}\right), \tag{2a}$$

$$\boldsymbol{E}^{\mathrm{e}} = \frac{1}{2}\left(\boldsymbol{F}^{\mathrm{e}\mathrm{T}}\boldsymbol{F}^{\mathrm{e}} - \boldsymbol{I}\right), \tag{2b}$$

$$\boldsymbol{E}^{\mathrm{p}} = \frac{1}{2}\left(\boldsymbol{F}^{\mathrm{p}\mathrm{T}}\boldsymbol{F}^{\mathrm{p}} - \boldsymbol{I}\right). \tag{2c}$$

Therefore, the total strain tensor is expressed as

$$\begin{aligned}\boldsymbol{E} &= \frac{1}{2}\left[\left(\boldsymbol{F}^{*\mathrm{T}}\boldsymbol{F}^{\mathrm{e}\mathrm{T}}\boldsymbol{F}^{\mathrm{p}\mathrm{T}}\boldsymbol{F}^{\mathrm{p}}\boldsymbol{F}^{\mathrm{e}}\boldsymbol{F}^{*}\right) - \boldsymbol{I}\right] \\ &= \frac{1}{2}\left(\boldsymbol{F}^{*\mathrm{T}}\boldsymbol{F}^{\mathrm{e}\mathrm{T}}\boldsymbol{F}^{\mathrm{e}}\boldsymbol{F}^{*} - \boldsymbol{I}\right) + \boldsymbol{F}^{*\mathrm{T}}\boldsymbol{F}^{\mathrm{e}\mathrm{T}}\boldsymbol{E}^{\mathrm{p}}\boldsymbol{F}^{\mathrm{e}}\boldsymbol{F}^{*} \\ &= \boldsymbol{E}^{*} + \boldsymbol{F}^{*\mathrm{T}}\boldsymbol{E}^{\mathrm{e}}\boldsymbol{F}^{*} + \boldsymbol{F}^{*\mathrm{T}}\boldsymbol{F}^{\mathrm{e}\mathrm{T}}\boldsymbol{E}^{\mathrm{p}}\boldsymbol{F}^{\mathrm{e}}\boldsymbol{F}^{*}.\end{aligned} \tag{3}$$

Based on the polar decomposition of the tensor, the deformation gradients $\boldsymbol{F}^{*}$ and $\boldsymbol{F}^{\mathrm{e}}$ are written respectively as

$$\boldsymbol{F}^{*} = \boldsymbol{R}^{*}\boldsymbol{U}^{*}, \tag{4}$$

$$\boldsymbol{F}^{\mathrm{e}} = \boldsymbol{R}^{\mathrm{e}}\boldsymbol{U}^{\mathrm{e}}, \tag{5}$$

where $\boldsymbol{R}^{*}$ and $\boldsymbol{R}^{\mathrm{e}}$ are the rotation tensors, and $\boldsymbol{U}^{*}$ and $\boldsymbol{U}^{\mathrm{e}}$ are the stretch tensors.

Assuming that $\boldsymbol{R}^{*} = \boldsymbol{I}$, $\boldsymbol{R}^{\mathrm{e}} = \boldsymbol{I}$, the total strain tensor is expressed as

$$\boldsymbol{E} = \boldsymbol{E}^{*} + \boldsymbol{U}^{*}\boldsymbol{E}^{\mathrm{e}}\boldsymbol{U}^{*} + \boldsymbol{U}^{*}\boldsymbol{U}^{\mathrm{e}}\boldsymbol{E}^{\mathrm{p}}\boldsymbol{U}^{\mathrm{e}}\boldsymbol{U}^{*}. \tag{6}$$

Based on Eqs. (2a), (2b), (4) and (5), we can obtain

$$\boldsymbol{E}^{*} = \frac{1}{2}\left[\left(\boldsymbol{U}^{*}\right)^{2} - \boldsymbol{I}\right], \tag{7a}$$

$$\boldsymbol{E}^{\mathrm{e}} = \frac{1}{2}\left[\left(\boldsymbol{U}^{\mathrm{e}}\right)^{2} - \boldsymbol{I}\right]. \tag{7b}$$

The Taylor expansions of $\boldsymbol{U}^{*}$ and $\boldsymbol{U}^{\mathrm{e}}$ are

$$\boldsymbol{U}^{*} = (\boldsymbol{I} + 2\boldsymbol{E}^{*})^{1/2} = \boldsymbol{I} + \boldsymbol{E}^{*} - \frac{1}{2}\left(\boldsymbol{E}^{*}\right)^{2} + \cdots, \tag{8a}$$

$$\boldsymbol{U}^{\mathrm{e}} = (\boldsymbol{I} + 2\boldsymbol{E}^{\mathrm{e}})^{1/2} = \boldsymbol{I} + \boldsymbol{E}^{\mathrm{e}} - \frac{1}{2}\left(\boldsymbol{E}^{\mathrm{e}}\right)^{2} + \cdots. \tag{8b}$$

If the thermal strain tensor $\boldsymbol{E}^*$ and elastic strain tensor $\boldsymbol{E}^{\mathrm{e}}$ are small, we can obtain

$$\boldsymbol{U}^* \cong \boldsymbol{I} + \boldsymbol{E}^*, \tag{9a}$$

$$\boldsymbol{U}^{\mathrm{e}} \cong \boldsymbol{I} + \boldsymbol{E}^{\mathrm{e}}, \tag{9b}$$

and

$$\boldsymbol{U}^* \cong \boldsymbol{I}, \tag{10a}$$

$$\boldsymbol{U}^{\mathrm{e}} \cong \boldsymbol{I}. \tag{10b}$$

Then, the total strain tensor takes

$$\boldsymbol{E} = \boldsymbol{E}^* + \boldsymbol{E}^{\mathrm{e}} + \boldsymbol{E}^{\mathrm{p}}. \tag{11}$$

Equation (11) is a new strain tensor expression of the elastic and plastic deformation at the finite temperature, and it extends the kinematical theory of the elastic-plastic deformation of the crystal.

2.2 Thermal strain

When an undeformed body is heated up from temperature T_0 to T, the thermal strain ε_T is given by [36]

$$\varepsilon_T = \int_{T_0}^{T} \alpha \mathrm{d}T, \tag{12}$$

where T_0 is the reference temperature. α is the coefficient of thermal expansion, which can be obtained from the experimental results [37] and also can be calculated by the theoretical method [38].

For the metal material, the thermal strain tensor $\boldsymbol{E}^*$ is as

$$\boldsymbol{E}^* = \begin{bmatrix} \varepsilon_T & 0 & 0 \\ 0 & \varepsilon_T & 0 \\ 0 & 0 & \varepsilon_T \end{bmatrix}. \tag{13}$$

The calculations for lattice constant $r^{(0)}(T)$ at temperature T were given by Jiang [39] as follows:

$$r^{(0)}(T) = r^{(0)}(T_0)\left(1 + \int_{T_0}^{T} \alpha \mathrm{d}T\right). \tag{14}$$

2.3 Thermo-elasticity constitutive equation for single crystals

The second Piola–Kirchhoff stress is expressed as

$$\boldsymbol{S} = \frac{\partial W}{\partial \boldsymbol{E}^{\mathrm{e}}} = \frac{1}{V^*}\left[\frac{\partial U_{\mathrm{tot}}\left(\boldsymbol{E}^{\mathrm{e}}\right)}{\partial \boldsymbol{E}^{\mathrm{e}}}\right], \tag{15}$$

where V^* is the volume at the first intermediate configuration as shown in Fig. 1b, U_{tot} is the total potential energy of the system.

The rate of the second Piola–Kirchhoff stress takes

$$\begin{aligned} \dot{\boldsymbol{S}} &= \frac{1}{V^*}\left[\frac{\partial U_{\mathrm{tot}}^2\left(\boldsymbol{E}^{\mathrm{e}}\right)}{\partial \boldsymbol{E}^{\mathrm{e}} \partial \boldsymbol{E}^{\mathrm{e}}}\right] : \dot{\boldsymbol{E}}^{\mathrm{e}} \\ &= \frac{1}{V^*}\left[\frac{\partial U_{\mathrm{tot}}^2\left(\boldsymbol{E}^{\mathrm{e}}\right)}{\partial \boldsymbol{E}^{\mathrm{e}} \partial \boldsymbol{E}^{\mathrm{e}}}\right] : \left(\dot{\boldsymbol{E}} - \dot{\boldsymbol{E}}^{\mathrm{p}} - \dot{\boldsymbol{E}}^*\right). \end{aligned} \tag{16}$$

Equation (16) can be written as

$$\dot{\boldsymbol{S}} = \boldsymbol{C}^{\mathrm{sig}} : \dot{\boldsymbol{E}}^{\mathrm{e}}, \tag{17}$$

where $\boldsymbol{C}^{\mathrm{sig}}$ is the thermo-elastic stiffness tensor for single crystals. And the change of lattice constant with temperature is considered in the calculation of total potential energy U_{tot}. So the stiffness $\boldsymbol{C}^{\mathrm{sig}}$ changes with temperature.

The constitutive equation (16) is established by the rate of the second Piola–Kirchhoff stress and the rate of the Green strain based on the new deformation gradient decomposition. Since the decomposition is obtained under the condition that the elastic and thermal strain is small (Eqs. (9–10)), the constitutive equation can also be applied under this condition. Although the plastic strain of metal material always exceeds small deformation range, the decomposition is available because the elastic and thermal strain is small enough.

3 Thermo-elasto-plasticity constitutive relationship for polycrystal

3.1 Thermo-elastic constants for polycrystal

Polycrystalline material can be considered an aggregate of randomly oriented single crystals. The orientation of a crystallite in a polycrystalline sample is specified by means of Euler angles (θ, φ, ψ) [40]. The component of the thermo-elastic stiffness tensor for the polycrystalline C_{ijkl}^{pol} can be obtained by

$$\begin{aligned} C_{ijkl}^{\mathrm{pol}} = \int_0^{\pi}\int_0^{2\pi}\int_0^{2\pi} &\left(R_{im}\right)^{-1}\left(R_{jn}\right)^{-1}\left(R_{kp}\right)^{-1}\left(R_{lq}\right)^{-1} \\ &\times C_{mnpq}^{\mathrm{sig}} f\left(\theta, \varphi, \psi\right) \sin\theta \mathrm{d}\psi \mathrm{d}\varphi \mathrm{d}\theta, \end{aligned} \tag{18}$$

where C_{mnpq}^{sig} is the component of thermo-elastic stiffness tensor for the single crystals, which can be obtained by Eq. (17), $\boldsymbol{R}$ is the rotation tensor described by the Euler angles, and its expression is given by Reo [40], R_{ij} is the component of $\boldsymbol{R}$, and $f\left(\theta, \varphi, \psi\right)$ is the crystalline orientation distribution function in the polycrystalline sample. This satisfies

$$\int_0^{\pi}\int_0^{2\pi}\int_0^{2\pi} f\left(\theta, \varphi, \psi\right) \sin\theta \mathrm{d}\psi \mathrm{d}\varphi \mathrm{d}\theta = 1. \tag{19}$$

Then, assuming that crystalline orientations satisfy the uniform distribution, $f(\theta, \varphi, \psi)$ would be constant as:

$$f(\theta, \varphi, \psi) = \frac{1}{8\pi^2}. \tag{20}$$

The component of the thermo-elastic stiffness tensor for the polycrystal is written as

$$\begin{aligned} &C^{\text{pol}}_{ijkl} \\ &= \frac{1}{8\pi^2}\int_0^{\pi}\int_0^{2\pi}\int_0^{2\pi} (R_{im})^{-1}\left(R_{jn}\right)^{-1}\left(R_{kp}\right)^{-1}\left(R_{lq}\right)^{-1} \\ &\quad \times C^{\text{sig}}_{mnpq}\sin\theta \mathrm{d}\psi \mathrm{d}\varphi \mathrm{d}\theta. \end{aligned} \tag{21}$$

For the single crystals of cubic metals, there are three independent elastic constants: C^{sig}_{1111}, C^{sig}_{1122}, C^{sig}_{1212}, and the elastic constants of polycrystalline cubic materials are calculated as

$$C^{\text{pol}}_{1111} = 0.6C^{\text{sig}}_{1111} + 0.4(C^{\text{sig}}_{1122} + 2C^{\text{sig}}_{1212}), \tag{22a}$$
$$C^{\text{pol}}_{1122} = 0.2C^{\text{sig}}_{1111} + 0.8C^{\text{sig}}_{1122} - 0.4C^{\text{sig}}_{1212}, \tag{22b}$$
$$C^{\text{pol}}_{1212} = 0.2C^{\text{sig}}_{1111} - 0.2C^{\text{sig}}_{1212} + 0.6C^{\text{sig}}_{1212}. \tag{22c}$$

While there are five independent elastic constants for the single crystals of hexagonal metals: C^{sig}_{1111}, C^{sig}_{3333}, C^{sig}_{1122}, C^{sig}_{1133}, C^{sig}_{1212}, C^{sig}_{1313}. The elastic constants of polycrystalline hexagonal materials are calculated as:

$$\begin{aligned} C^{\text{pol}}_{1111} &= 0.533C^{\text{sig}}_{1111} + 0.2C^{\text{sig}}_{3333} \\ &\quad + 0.266\left(C^{\text{sig}}_{1133} + 2.0C^{\text{sig}}_{1313}\right), \end{aligned} \tag{23a}$$
$$\begin{aligned} C^{\text{pol}}_{3333} &= 0.533C^{\text{sig}}_{1111} + 0.2C^{\text{sig}}_{3333} \\ &\quad + 0.266\left(C^{\text{sig}}_{1133} + 2.0C^{\text{sig}}_{1313}\right), \end{aligned} \tag{23b}$$
$$\begin{aligned} C^{\text{pol}}_{1122} &= 0.0667\left(C^{\text{sig}}_{1111} + C^{\text{sig}}_{3333}\right) + 0.333C^{\text{sig}}_{1122} \\ &\quad + 0.533C^{\text{sig}}_{1133} - 0.2668C^{\text{sig}}_{1313}, \end{aligned} \tag{23c}$$
$$\begin{aligned} C^{\text{pol}}_{1133} &= 0.0667\left(C^{\text{sig}}_{1111} + C^{\text{sig}}_{3333}\right) + 0.333C^{\text{sig}}_{1122} \\ &\quad + 0.533C^{\text{sig}}_{1133} - 0.2668C^{\text{sig}}_{1313}, \end{aligned} \tag{23d}$$
$$\begin{aligned} C^{\text{pol}}_{1313} &= 0.233c_{1111} + 0.0667C^{\text{sig}}_{3333} - 0.1667C^{\text{sig}}_{1122} \\ &\quad - 0.133C^{\text{sig}}_{1133} + 0.4C^{\text{sig}}_{1313}, \end{aligned} \tag{23e}$$
$$\begin{aligned} C^{\text{pol}}_{1212} &= \frac{1}{2}\left(C^{\text{pol}}_{1111} - C^{\text{pol}}_{1122}\right) \\ &= 0.233C^{\text{sig}}_{1111} + 0.0667C^{\text{sig}}_{3333} \\ &\quad - 0.1667C^{\text{sig}}_{1122} - 0.133C^{\text{sig}}_{1133} + 0.4C^{\text{sig}}_{1313}. \end{aligned} \tag{23f}$$

From Eqs. (23a)–(23f), it can be found that though the single crystals of hexagonal metals are anisotropic, there also are three independent elastic constants of polycrystalline hexagonal materials. This result is due to the assumption that the crystalline orientations satisfy uniform distribution in the polycrystalline sample.

Based on the above derivation, we are able to determine the rate of the second Piola–Kirchhoff stress of the polycrystalline material as

$$\dot{\boldsymbol{S}} = \boldsymbol{C}^{\text{pol}} : \dot{\boldsymbol{E}}^{\text{epol}}, \tag{24}$$

where $\dot{\boldsymbol{E}}^{\text{epol}}$ is the rate of the Green strain for the polycrystalline material.

3.2 Plastic constitutive equation for polycrystal

In order to determine the relationship between the plastic strain, and the stress at a given temperature, the power law of the macroscopic uniaxial strain–stress curve is adopted, and has been effectively adopted by the theoretical model [27,31,32,41]:

$$\sigma = \begin{cases} c\varepsilon^m, & \sigma \geq \sigma_{\text{ys}} \\ E'\varepsilon, & \sigma < \sigma_{\text{ys}} \end{cases}, \tag{25}$$

where c and m are parameters, E' is secant modulus of elasticity, and σ_{ys} is yield stress, which can be obtained by

$$\sigma_{\text{ys}} = c\varepsilon^m_{\text{ys}} = E'\varepsilon_{\text{ys}}, \tag{26}$$

where ε_{ys} is yield strain, which remains unchanged for the same material; then Eq. (25) can be written as follows:

$$\frac{\sigma}{\sigma_{\text{ys}}} = \begin{cases} \left(\dfrac{\varepsilon}{\varepsilon_{\text{ys}}}\right)^m, & \sigma \geq \sigma_{\text{ys}} \\ \dfrac{\varepsilon}{\varepsilon_{\text{ys}}}, & \sigma < \sigma_{\text{ys}} \end{cases}. \tag{27}$$

In Eq. (27), when the yield stress σ_{ys} and parameter m are determined at a given temperature, the stress–strain curve can then be obtained.

With consideration to the yield stress always changing with temperature, and in order to describe the temperature effects on the yield stress, we proposed the exponential curve based on the previous experiment and theoretical investigations as:

$$\sigma_{\text{ys}} = \sigma^0_{\text{ys}}\mathrm{e}^{-\beta T^*}, \tag{28}$$

where, $T^* = \frac{T}{T_0} - 1$, and T_0 is the reference temperature, σ^0_{ys} is the yield stress at reference temperature, and β is parameter which reflects the change of yield stress with temperature.

When, $\sigma \geq \sigma_{\text{ys}}$ (T), the stress is obtained by:

$$\sigma = \left(\frac{\varepsilon}{\varepsilon_{\text{ys}}}\right)^m \sigma^0_{\text{ys}}\mathrm{e}^{-\beta T^*}. \tag{29}$$

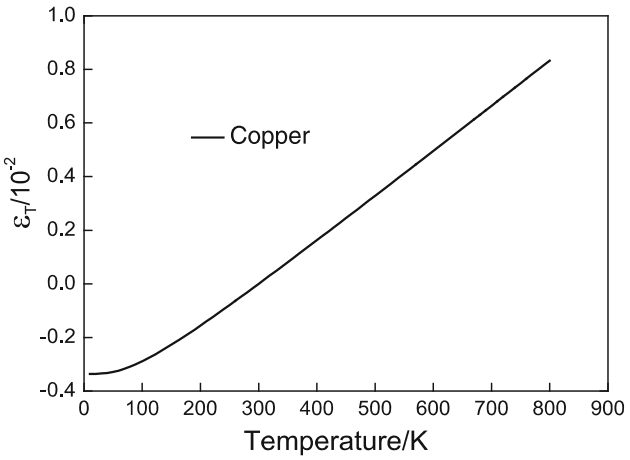

Fig. 2 Thermal strain of copper

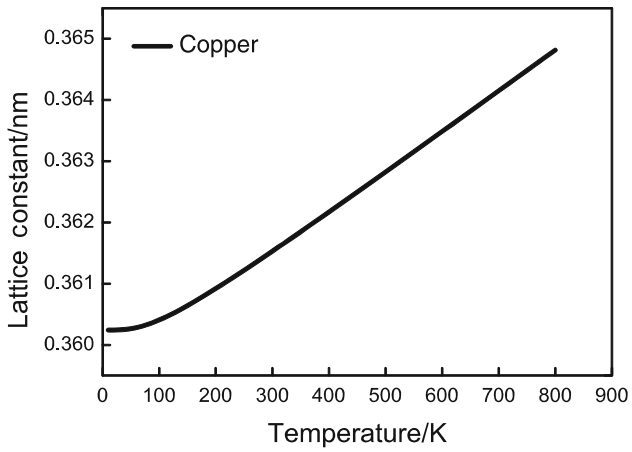

Fig. 3 Lattice constants of copper

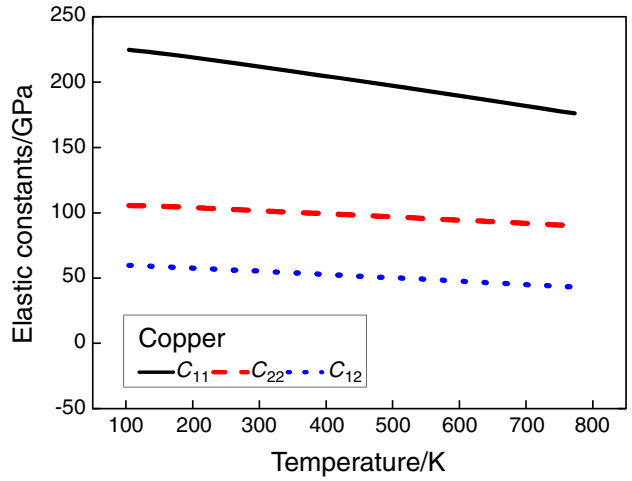

Fig. 4 Elastic constants of copper

4 Calculation results

In this study, the uniaxial stress–strain curves of FCC polycrystalline copper and HCP polycrystalline magnesium at various temperatures are calculated based on the present model, and the calculation results are compared with the experiment results [3,5,6].

4.1 FCC polycrystalline copper

The experimental results for the quasi-static uniaxial stress–strain curves of polycrystalline copper from 77 to 764 K were obtained by Roberts and Bergström [6].

4.1.1 Thermal strain and lattice constants for copper

The thermal strain and lattice constants at different temperatures are calculated based on Eqs. (12) and (14), respectively, and the thermal expansion α in Eqs. (12) and (14) is obtained from the experimental results [37]. Figures 2 and 3 show the thermal strain and the lattice constant versus temperature for copper. The thermal strain at room temperature is set as zero.

4.1.2 Elastic constants for copper

For copper, the EAM potential proposed by Mishin [42] is adopted to calculate the potential energy U_{tot} in Eq. (16). The change of lattice constant with temperature is considered in the calculation of thermo-elastic stiffness tensor [Eq. (17)], and the elastic constants of the polycrystalline copper at different temperatures can be easily obtained (Fig. 4).

4.1.3 Determination of calculated parameters for copper

For copper, the reference temperature is 293 K and yield strain ε_{ys} is 0.2 %. Based on Eq. (29), only three parameters are required: σ_{ys}^0, β, and m. The yield stress σ_{ys}^0 and parameter m are determined firstly by the stress–strain curve at 293 K. Then, from another stress–strain curve at a different temperature, the parameter β can be obtained. Figure 5 is the calculated curve of the yield stress versus the temperature for copper, which agrees well with the experimental results. And the calculated parameters for copper are shown in Table 1.

4.1.4 Calculated results for copper

Figure 6a–6c is the comparison of the uniaxial stress–strain curves for copper between the simulation and the experimental results at different temperatures (77–764 K). It can be found that the present model can potentially describe the behavior of the FCC polycrystalline copper effectively.

4.2 HCP polycrystalline magnesium

The experimental results of the magnesium come from data of two different studies: low and medium temperatures [3]: 77–523 K; high temperatures [5]: 675–870 K. Therefore, the

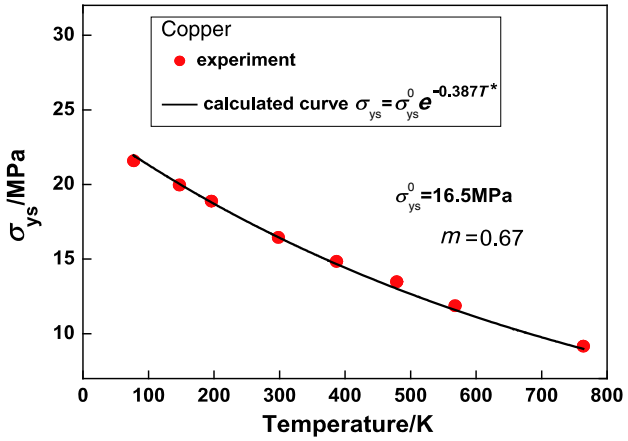

Fig. 5 Comparison of yield stress for copper between the calculated curve and experimental data at different temperatures

Table 1 Calculated parameters for copper

T (K)	σ_{ys}^{0} (MPa)	β	m
77–764	16.5	0.387	0.67

reference temperature is 293 K for low and medium temperatures, and 675 K for high temperatures, and the yield strain ε_{ys} is 0.05 %.

Based on previous investigations regarding magnesium [43], it can be determined that the low symmetry of the crystallographic structure, as well as the twinning behavior, would make the plastic deformation of the HCP polycrystalline more complicated. In comparing the two groups of experimental results, we found that the temperature effects on the plastic behavior at lower temperatures are more difficult to describe. Therefore, we adopted a special handling in the calculation of the magnesium at the low and medium temperatures.

4.2.1 Thermal strain and lattice constants for magnesium

The thermal strain and lattice constants for magnesium are obtained by the same method as copper, and the results are shown in the Figs. 7 and 8.

4.2.2 Elastic constants for magnesium

For magnesium, the EAM potential proposed by Zhou [44] is adopted to calculate the potential energy. The elastic constants at different temperatures for magnesium are as shown in Fig. 9.

4.2.3 Determination of calculated parameters for magnesium at high temperature

Similar to copper, the calculated parameters for magnesium at high temperatures is determined by two experimental stress–strain curves [5]. The calculated curve of the yield stress versus temperature for magnesium at high tempera-

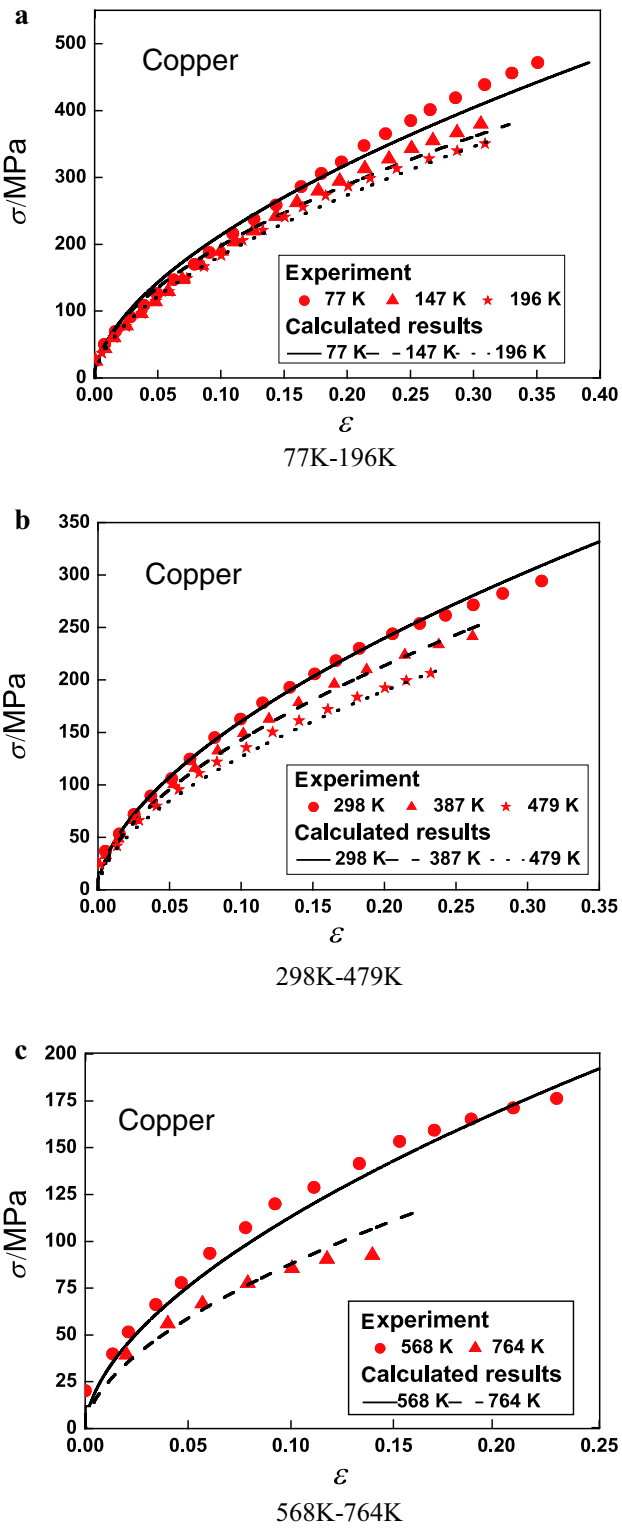

Fig. 6 Comparisons of uniaxial stress–strain curves for copper between the simulation and experiment results at different temperatures. **a** 77–196 K. **b** 298–479 K. **c** 568–764 K

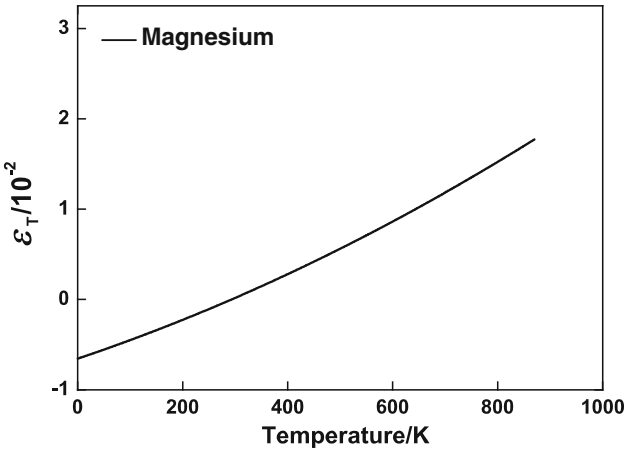

Fig. 7 Thermal strain of magnesium

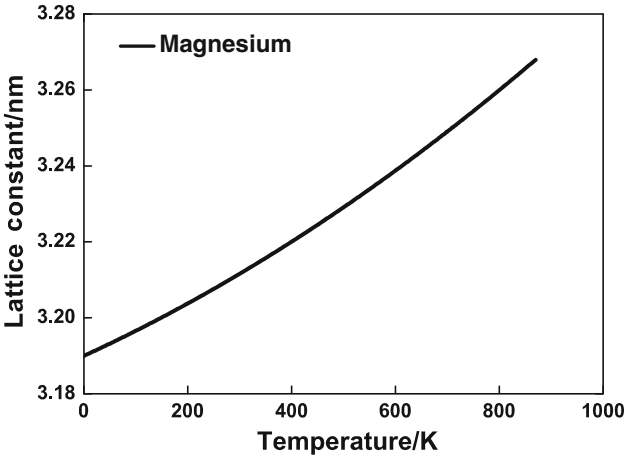

Fig. 8 Lattice constants of magnesium

ture is as shown in Fig. 10. The calculated parameters are illustrated in Table 2.

4.2.4 Calculated results for magnesium at high temperature

Figure 11a–11b shows the comparison of the uniaxial stress–strain curves of the simulation and experiment results at different temperatures for copper (675–870 K).

4.2.5 Determination of calculated parameters for magnesium at low and medium temperatures

From the stress–strain curves of the experiment [3], it can be determined that the plastic deformation of the HCP polycrystalline magnesium at low and medium temperatures appears to be more complicated than the above calculated results. If the parameter m remains unchanged at different temperatures, we are unable to obtain the correct calculated results. In order to describe accurately the temperature effects on the hardening behavior for magnesium at low and medium

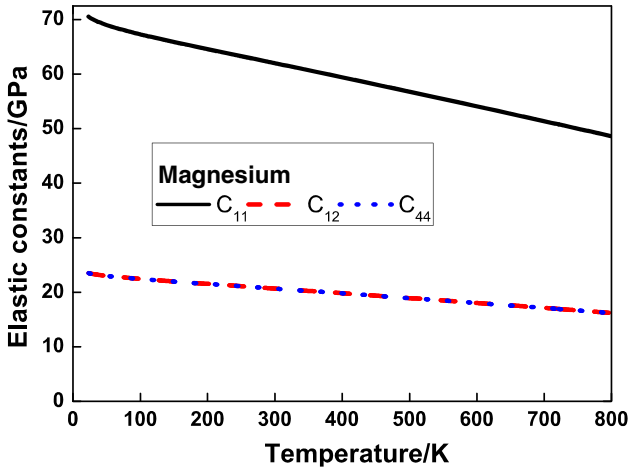

Fig. 9 Elastic constants of magnesium

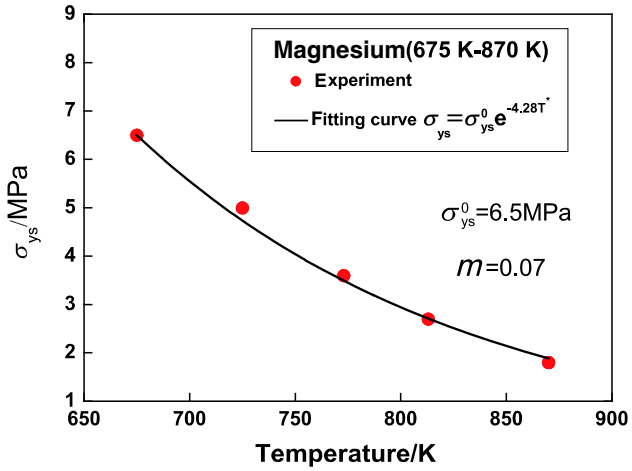

Fig. 10 Comparison of yield stress for magnesium between the calculated curve and experimental data at high temperatures

Table 2 Calculated parameters for magnesium at high temperature

T (K)	σ_{ys}^0 (MPa)	β	m
675–870	6.5	4.28	0.07

temperatures, we adopted a bilinear function to describe the change of parameter m with the various temperatures as

$$m = m_0(1 + aT^* + bT^{*2}), \tag{30}$$

where m_0 is the value of m at reference temperature, and a and b are parameters.

Then, the yield stress σ_{ys}^0 and m_0 are first determined by the stress–strain curve at the reference temperatures. The parameters a and b can be obtained by another two stress–strain curves at different temperatures. Meanwhile, the parameter β can be obtained. Figure 12 is the comparison of the calculated curve for m with the experimental results at different temperatures. Figure 13 is the comparison of the calculated

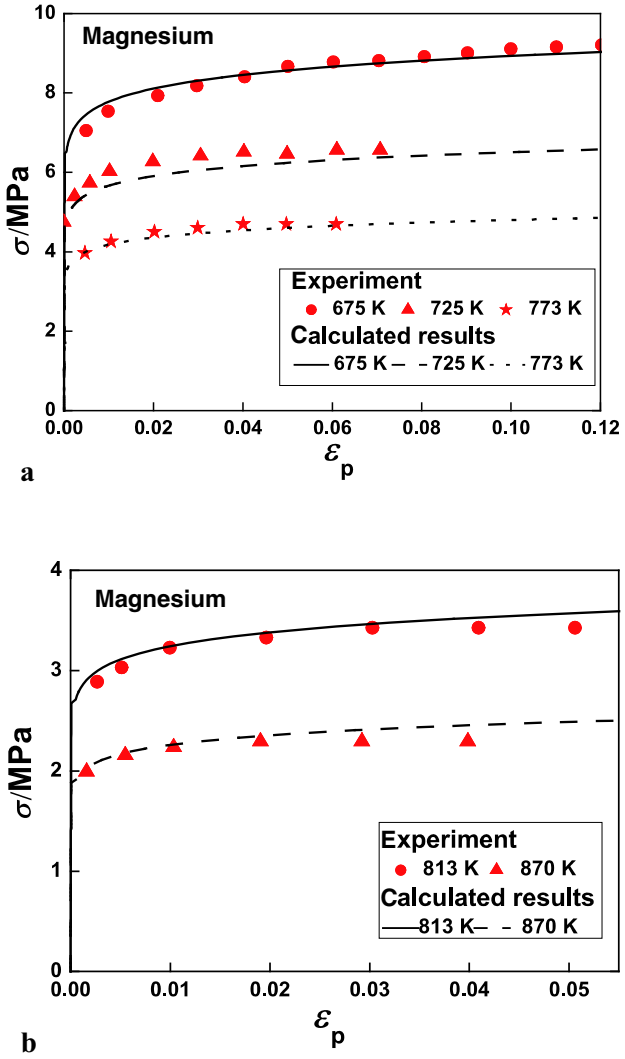

Fig. 11 Comparisons of uniaxial stress–strain curves for magnesium between the simulation and experiment results at high temperature. **a** 675–773 K. **b** 813–870 K

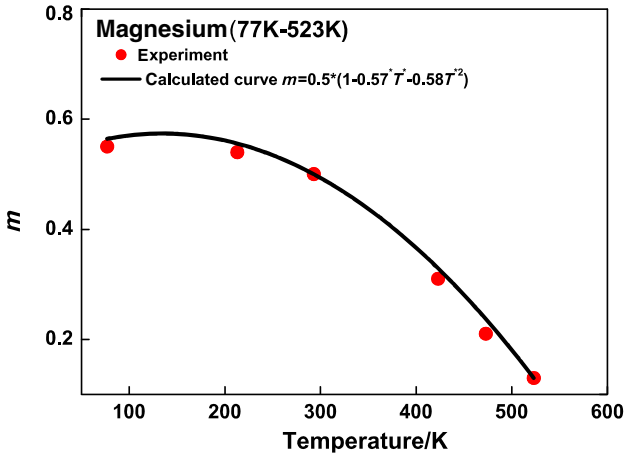

Fig. 12 Comparison of parameter m for magnesium between the calculated curve and experimental data at low and medium temperatures

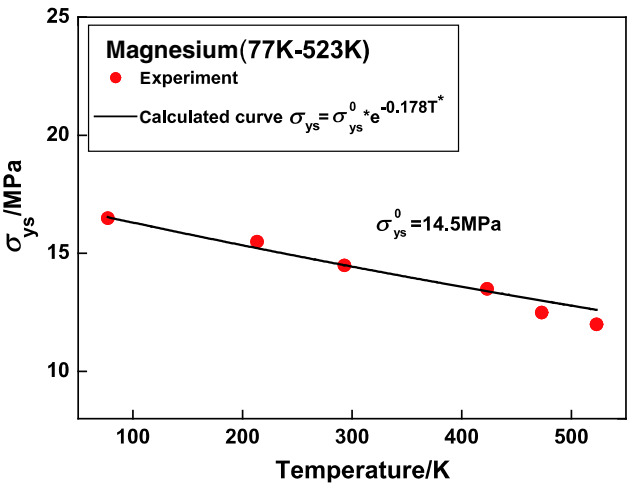

Fig. 13 Comparison of yield stress for magnesium between the calculated curve and experimental data at low and medium temperatures

curve for yield stress σ_{ys} with the experimental results. It can be seen that the calculated curves agree well with the experimental results.

The calculated parameters for magnesium at low and medium temperatures are as shown in Table 3.

4.2.6 Calculated results for magnesium at low and medium temperatures

Figure 14a, 14b is the comparison of the uniaxial stress–strain curves for the magnesium between the calculation and the experimental results at low and medium temperatures (77–523 K). It can be determined that the present model can potentially describe the behavior of the HCP polycrystalline magnesium efficiently.

5 Discussion

When compared with the kinematical theory described by Asaro [33,34], whose deformation gradient is written as $\boldsymbol{F} = \boldsymbol{F}^{\mathrm{e}}\boldsymbol{F}^{\mathrm{p}}$, the new decomposition of the total deformation gradient is effective when the constitutive equation is applied to the thermal strain. Moreover, the new decomposition equation $\boldsymbol{F} = \boldsymbol{F}^{\mathrm{p}}\boldsymbol{F}^{\mathrm{e}}\boldsymbol{F}^{*}$ in this study is able to obtain the simple strain tensor in Eq. (11), which is more favorable than the other decomposition expressions. Then, based on the new decomposition, we established the constitutive equation for crystals. However, the new decomposition is established under the condition that the elastic and thermal strain is small enough, so the new constitutive equation is also applicative in this condition.

The plastic deformation and the decrease of yield stress with temperature are reflected by simple power and exponential relationships respectively. The calculation is more

Table 3 Calculated parameters for magnesium at low and medium temperatures

T (K)	σ_{ys}^0 (MPa)	β
77–523	14.5	0.178
m_0	a	b
0.5	−0.57	−0.58

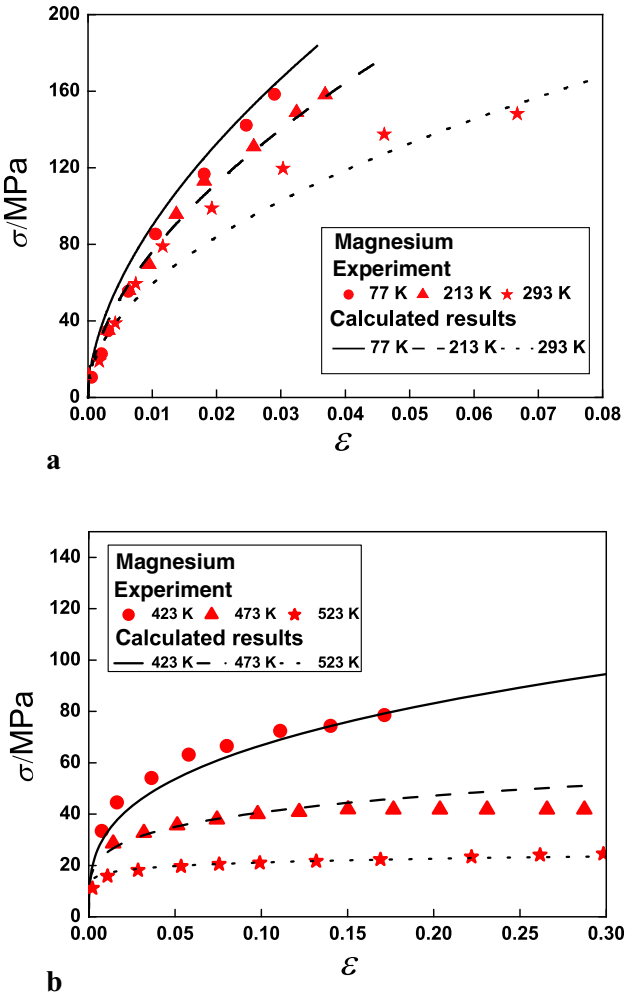

Fig. 14 Comparisons of uniaxial stress–strain curves for magnesium between the simulation and experimental results at low and medium temperatures. **a** 77–293 K. **b** 423–523 K

concise, and the parameters can be determined by only two or three uniaxial stress–strain curves at different temperatures. Therefore, it is easy to describe the temperature effects on the thermo-elasto-plasticity behaviors of the materials.

By comparing the calculations between the FCC polycrystalline copper and the HCP polycrystalline magnesium, it can be found that the material behaviors of the magnesium at low and medium temperature is the more complex. The parameter m drops off for the magnesium at low and medium temperatures, which is described by a bilinear function in Eq. (30). Based on many previous theories investigated in the literature [45–48], these phenomena can be explained by the differences of the crystallographic structure, the interaction among grains, and the plastic mechanism between the FCC (or BCC) and the HCP polycrystalline metals. First of all, the FCC (or BCC) polycrystalline metals keep the symmetry of the crystallographic structure, and their slip systems for the dislocation motion have roughly equal resistance. Therefore, the plastic deformation in most FCC materials is dominated by crystallographic slip. However, due to the low symmetry of the crystallographic structure of the HCP polycrystalline metals, one must carefully take into account the details of the stress/strain variations from the grain, and the interaction between the crystals and grains. Also, different types of slip systems exist, and both slip and twinning contribute to the plastic deformation in the HCP crystals [17,49,50]. As the temperature increases, the plastic deformation transits from being twinning dominated to a combination of slip and twinning [49] or slip dominated [43]. All the above factors show that the simulation of the plastic behaviors at different temperatures for the HCP is more difficult than for the FCC. In this paper, we provide a concise method to reflect the different of macroscopic behavior of the FCC and the HCP polycrystalline materials.

6 Conclusion

In this study, a new thermo-elasto-plasticity constitutive theory is proposed to investigate the behaviors of polycrystalline metals. First of all, the present new decomposition of the deformation gradient is effective when applied to the thermal strain, and the calculation of the total strain is simpler and more explicit. Then, the constitutive equations of a single crystal and polycrystal are established, and we provide a new method to describe the temperature effects on the yield stress, as well as the hardening behavior of the FCC and HCP polycrystalline. Lastly, the comparisons between the calculations and the experimental results show that the present model can potentially accurately reflect the behavior of the polycrystalline metals at different temperatures with a concise and clear calculation process.

Acknowledgments This work is supported by the National Natural Science Foundation of China (Grants 11021262, 11172303, 11132011) and National Basic Research Program of China through 2012CB937500.

References

1. Chen, S.R., Kocks, U.: High-Temperature Plasticity in Copper Polycrystals. Los Alamos National Laboratory, Los Alamos (1991)
2. Nemat-Nasser, S., Li, Y.: Flow stress of fcc polycrystals with application to OFHC Cu. Acta Mater. **46**, 565–577 (1998)

3. Ono, N., Nowak, R., Miura, S.: Effect of deformation temperature on Hall–Petch relationship registered for polycrystalline magnesium. Mater. Lett. **58**, 39–43 (2004)
4. Lennon, A., Ramesh, K.: The influence of crystal structure on the dynamic behavior of materials at high temperatures. Int. J. Plast. **20**, 269–290 (2004)
5. Vagarali, S.S., Langdon, T.G.: Deformation mechanisms in hcp metals at elevated temperatures–I. Creep behavior of magnesium. Acta Metall. **29**, 1969–1982 (1981)
6. Roberts, W., Bergström, Y.: The stress–strain behaviour of single crystals and polycrystals of face-centered cubic metals—a new dislocation treatment. Acta Metall. **21**, 457–469 (1973)
7. Viguier, B., Kruml, T., Martin, J.L.: Loss of strength in Ni3Al at elevated temperatures. Philos. Mag. **86**, 4009–4021 (2006)
8. Prasad, Y.V.R.K., Rao, K.P.: Kinetics of high-temperature deformation of polycrystalline OFHC copper and the role of dislocation core diffusion. Philos. Mag. **84**, 3039–3050 (2004)
9. Taylor, G.I.: Plastic strain in metals. J. Inst. Met. **62**, 307–324 (1938)
10. Hill, R.: Continuum micro-mechanics of elastoplastic polycrystals. J. Mech. Phys. Solids **13**, 89–101 (1965)
11. Roters, F., Eisenlohr, P., Hantcherli, L., et al.: Overview of constitutive laws, kinematics, homogenization and multiscale methods in crystal plasticity finite-element modeling: Theory, experiments, applications. Acta Mater. **58**, 1152–1211 (2010)
12. Raabe, D., Mao, W.: Experimental investigation and simulation of the texture evolution during rolling deformation of an intermetallic Fe-28 at.% A1–2 at.% Cr polycrystal at elevated temperatures. Philos. Mag. A **71**, 805–813 (1995)
13. Kocks, U.: The relation between polycrystal deformation and single-crystal deformation. Metall. Mater. Trans. **1**, 1121–1143 (1970)
14. Balasubramanian, S., Anand, L.: Elasto-viscoplastic constitutive equations for polycrystalline fcc materials at low homologous temperatures. J. Mech. Phys. Solids **50**, 101–126 (2002)
15. Hutchinson, J.: Bounds and self-consistent estimates for creep of polycrystalline materials. Proc. R. Soc. Lond. A **348**, 101–127 (1976)
16. Landis, C.M., McMeeking, R.M.: A self-consistent constitutive model for switching in polycrystalline barium titanate. Ferroelectrics **255**, 13–34 (2001)
17. Wang, H., Raeisinia, B., Wu, P., et al.: Evaluation of self-consistent polycrystal plasticity models for magnesium alloy AZ31B sheet. Int. J. Solids Struct. **47**, 2905–2917 (2010)
18. Agnew, S.R., Duygulu, Ö.: Plastic anisotropy and the role of non-basal slip in magnesium alloy AZ31B. Int. J. Plast. **21**, 1161–1193 (2005)
19. Askari, H., Young, J.P., Field, D.P., et al.: Prediction of flow stress and textures of AZ31 magnesium alloy at elevated temperature. Philos. Mag. **94**, 3353–3367 (2014)
20. Turner, P.A., Tomé, C.N., Christodoulou, N., et al.: A self-consistent model for polycrystals undergoing simultaneous irradiation and thermal creep. Philos. Mag. A **79**, 2505–2524 (1999)
21. Beyerlein, I., Tomé, C.: A dislocation-based constitutive law for pure Zr including temperature effects. Int. J. Plast. **24**, 867–895 (2008)
22. Bower, A.F., Wininger, E.: A two-dimensional finite element method for simulating the constitutive response and microstructure of polycrystals during high temperature plastic deformation. J. Mech. Phys. Solids **52**, 1289–1317 (2004)
23. Agarwal, S., Briant, C.L., Krajewski, P.E., et al.: Experimental validation of two-dimensional finite element method for simulating constitutive response of polycrystals during high temperature plastic deformation. J. Mater. Eng. Perform. **16**, 170–178 (2007)
24. Ma, A., Roters, F.: A constitutive model for fcc single crystals based on dislocation densities and its application to uniaxial compression of aluminium single crystals. Acta Mater. **52**, 3603–3612 (2004)
25. Zamiri, A., Bieler, T., Pourboghrat, F.: Anisotropic crystal plasticity finite element modeling of the effect of crystal orientation and solder joint geometry on deformation after temperature change. J. Electron. Mater. **38**, 231–240 (2009)
26. Staroselsky, A., Anand, L.: A constitutive model for hcp materials deforming by slip and twinning: Application to magnesium alloy AZ31B. Int. J. Plast. **19**, 1843–1864 (2003)
27. Johnson, G. R., Cook W. H.: A constitutive model and data for metals subjected to large strains, high strain rates and high temperatures. In: Proceedings of the 7th International Symposium on Ballistics, The Hague (1983)
28. Zerilli, F.J., Armstrong, R.W.: Dislocationc-mechanicsc-based constitutive relations for material dynamics calculations. J. Appl. Phys. **61**, 1816–1825 (1987)
29. Khan, A.S., Huang, S.: Experimental and theoretical study of mechanical behavior of 1100 aluminum in the strain rate range $10^{-5} - 10^{4}\ S^{-1}$. Int. J. Plast. **8**, 397–424 (1992)
30. Khan, A.S., Liang, R.: Behaviors of three BCC metal over a wide range of strain rates and temperatures: experiments and modeling. Int. J. Plast. **15**, 1089–1109 (1999)
31. Khan, A.S., Yu, S., Liu, H.: Deformation induced anisotropic responses of Ti–6Al–4V alloy part II: A strain rate and temperature dependent anisotropic yield criterion. Int. J. Plast. **38**, 14–26 (2012)
32. Liang, R., Khan, A.S.: A critical review of experimental results and constitutive models for BCC and FCC metals over a wide range of strain rates and temperatures. Int. J. Plast. **15**, 963–980 (1999)
33. Asaro, R.J.: Crystal plasticity. J. Appl. Mech. **50**, 921–934 (1983)
34. Asaro, R.J., Rice, J.R.: Strain localization in ductile single crystals. J. Mech. Phys. Solids **25**, 309–338 (1977)
35. Hill, R.: Generalized constitutive relations for incremental deformation of metal crystals by multislip. J. Mech. Phys. Solids **14**, 95–102 (1966)
36. Liu, X.L., Tang, Q.H., Wang, T.C.: A continuum thermal stress theory for crystals based on interatomic potentials. Sci. China Phys. Mech. Astron. **57**, 1–10 (2014)
37. Nix, F.C., MacNair, D.: The thermal expansion of pure metals: Copper, gold, aluminum, nickel, and iron. Phys. Rev. **60**, 597–605 (1941)
38. Tang, Q., Wang, T., Shang, B., et al. Thermodynamic properties and constitutive relations of crystals at finite temperature. Sci. China Phys. Mech. Astron. **55**, 918–926 (2012)
39. Jiang, H., Huang, Y., Hwang, K.C.: A finite-temperature continuum theory based on interatomic potentials. J. Eng. Mater. Technol. **127**, 408–416 (2005)
40. Roe, R.J.: Description of crystallite orientation in polycrystalline materials. III. General solution to pole figure inversion. J. Appl. Phys. **36**, 2024–2031 (1965)
41. Khan, A.S., Yu, S.: Deformation induced anisotropic responses of Ti–6Al–4V alloy. Part I: Experiments. Int. J. Plast. **38**, 1–13 (2012)
42. Mishin, Y., Mehl, M., Papaconstantopoulos, D., et al. Structural stability and lattice defects in copper: Ab initio, tight-binding, and embedded-atom calculations. Phys. Rev. B **63**, 224106 (2001)
43. Barnett, M., Keshavarz, Z., Beer, A., et al.: Influence of grain size on the compressive deformation of wrought Mg-3Al-1Zn. Acta Mater. **52**, 5093–5103 (2004)
44. Zhou, X.W., Johnson, R.A., Wadley, H.N.G.: Misfit-energy-increasing dislocations in vapor-deposited CoFe/NiFe multilayers. Phys. Rev. B **69**, 144113 (2004)
45. Agnew, S.R., Brown, D.W., Tomé, C.N.: Validating a polycrystal model for the elastoplastic response of magnesium alloy AZ31 using in situ neutron diffraction. Acta Mater. **54**, 4841–4852 (2006)

46. Gehrmann, R., Frommert, M.M., Gottstein, G.: Texture effects on plastic deformation of magnesium. Mater. Sci. Eng. A **395**, 338–349 (2005)
47. Yoo, M.H., Lee, J.K.: Deformation twinning in h.c.p. metals and alloys. Philos. Mag. A **63**, 987–1000 (1991)
48. Matsunaga, T., Kameyama, T., Ueda, S., et al. Grain boundary sliding during ambient-temperature creep in hexagonal close-packed metals. Philos. Mag. **90**, 4041–4054 (2010)
49. Liu, Y., Wei, Y.: A polycrystal based numerical investigation on the temperature dependence of slip resistance and texture evolution in magnesium alloy AZ31B. Int. J. Plast. **55**, 80–93 (2014)
50. Knezevic, M., McCabe, R.J., Tomé, C.N., et al.: Modeling mechanical response and texture evolution of α-uranium as a function of strain rate and temperature using polycrystal plasticity. Int. J. Plast. **43**, 70–84 (2013)